RESEARCH ARTICLE

Local Response to Microneedle-Based Influenza Immunization in the Skin

Maria del Pilar Martin,[a] William C. Weldon,[a] Vladimir G. Zarnitsyn,[b] Dimitrios G. Koutsonanos,[a] Hamed Akbari,[c] Ioanna Skountzou,[a] Joshy Jacob,[a] Mark R. Prausnitz,[b] and Richard W. Compans[a]

Department of Microbiology and Immunology and Emory Vaccine Center, Emory University School of Medicine, Atlanta, Georgia, USA[a]; School of Chemical and Biomolecular Engineering, Georgia Institute of Technology, Atlanta, Georgia, USA[b]; and Department of Radiology and Imaging Sciences, Emory School of Medicine, Atlanta, Georgia, USA[c]

ABSTRACT **Microneedle patches (MN) provide a novel method of vaccine delivery to the skin with the objective of targeting the large network of resident antigen-presenting cells to induce an efficient immune response. Our previous reports demonstrated that cutaneous delivery of inactivated influenza virus-coated MN to mice protects against lethal infection. Protection is correlated with sustained levels of anti-influenza virus serum antibodies, hemagglutination inhibition titers, and robust cellular responses that are often stronger than those generated by intramuscular vaccination. Here we dissect the early events occurring in murine skin after microneedle delivery of inactivated influenza virus. We demonstrate correlation of immunization against influenza virus with a local increase of cytokines important for recruitment of neutrophils, monocytes and dendritic cells at the site of immunization. We also observed prolonged antigen deposition, and migration of matured dendritic cells bearing influenza virus antigen from the skin.**

IMPORTANCE **The immunological mechanisms by which MN vaccination confers protective immunity are not well understood. The present study provides a first analysis of the early immune events after microneedle-based vaccination.**

Received 12 January 2012 **Accepted** 2 February 2012 **Published** 6 March 2012

Citation del Pilar Martin M, et al. 2012. Local response to microneedle-based influenza immunization in the skin. mBio 3(2):e00012-12. doi:10.1128/mBio.00012-12.

Editor Jack Bennink, National Institute of Allergy and Infectious Diseases

Address correspondence to Richard W. Compans, rcompan@emory.edu.

Vaccination against infectious agents remains the most effective method of disease prevention and one of the most important health advances in history. Vaccines prevent or ameliorate infection based on two fundamental principles: the generation of a rapid and effective immune response, and long-lived specific immunity. Despite the success of vaccination, a number of challenging pathogens continue to elude complete protection by vaccines due to their rapid mutation capacity and/or the variety of subtypes that exist in nature. Due to the antigenic diversity observed among influenza virus strains and limited duration of the immune response to inactivated vaccines, annual vaccination is required (1). The influenza vaccine composition is determined every year based on the analysis of influenza surveillance activity reports, which help to estimate which strains of virus are expected to circulate in the human population (2). Efficacy of the inactivated influenza vaccine is correlated with seroconversion against the major influenza surface protein, the hemagglutinin (3, 4). Acceptable levels of hemagglutinin antibody titers are normally achieved by higher doses and/or multiple doses in individuals who have not been previously exposed to an influenza virus of the same subtype (5). Influenza vaccination could benefit from new vaccine formulations and novel vaccine delivery methods that provide an enhanced immune response.

Alternate routes of vaccination to the conventional intramuscular delivery have been found to produce enhanced immune responses, and in humans, a nasally administered live attenuated influenza vaccine has also proven to be effective (6). However, this vaccine is approved only for healthy individuals 2 through 49 years of age, which excludes those at highest risk for developing influenza-related complications, such as infants, elderly persons, and immunocompromised individuals (7). One very attractive and promising alternative route of immunization is the skin. In 2011, the U.S. Food and Drug Administration (FDA) approved the first dermally administered influenza vaccine for human use in the United States (8, 9). The skin is not merely a physical barrier; a large body of work has demonstrated that the skin is also a complex and active immune site. Intradermal delivery provides access to the dense network of antigen-presenting cells, including macrophages, Langerhans cells, and dermal dendritic cells (DC) present in the dermis and epidermis, which are crucial in the initiation of the adaptive immune response and provide a favorable site for immunization (10, 11).

Recent work from our laboratories and others has shown that vaccine delivery via the skin using metal microneedle patches (MN) coated with influenza antigens or dissolving microneedles with encapsulated inactivated influenza virus results in enhanced or equivalent protection compared to delivery via the conventional intramuscular or subcutaneous routes (12–16). Challenge studies in MN-immunized mice demonstrated complete protection against homosubtypic viruses. MN vaccination induced a broad spectrum of immune responses, including higher frequency of virus-specific $CD4^+$ and $CD8^+$ T cells, virus-specific antibody-

secreting cells in the lung, and induction of a broader IgG isotype profile compared to conventional intramuscular delivery. These adaptive immune responses are the result of orchestrated events initiated by the innate immune system, which plays a fundamental role in sensing microbes and danger signals through pattern recognition receptors (PRR) (17). The plasticity of DC subsets and the PPR responses have been described as key initiating factors that ultimately determine the quality of the adaptive immune response (18). Therefore, we investigated the early events after MN vaccination in order to gain new insights into the innate immunological mechanisms involved in MN delivery.

In this study we dissected the events that occur in the skin at early time points following influenza MN vaccination in mice. We analyzed the time course of antigen retention within the skin and the release of inflammatory cytokines mediated by MN insertion. Furthermore, we analyzed the egress of influenza antigen-bearing $CD11c^+$ DC from the skin and their phenotype. These results provide evidence of robust local innate immune responses generated by MN delivery to the skin, and may provide insight into how immune responses may differ depending on the vaccination route.

RESULTS

Cytokine and chemokine expression in the skin. After antigen is deposited within the skin, cytokines and their subsequent recruitment of immune cells at the site of delivery may play an important role in the robust adaptive immune response observed after MN vaccination. To evaluate the innate responses that occur locally after MN delivery, biopsies of tissue from the MN insertion site of mice immunized with inactivated influenza virus or mock immunized with uncoated microneedles were carried out and compared to naïve-skin biopsies. The biopsy samples were collected 6 h and 12 h postimmunization, and the levels of 31 murine cytokines were compared between the groups.

After MN vaccination, we observed significant increases in the levels of the cytokines interleukin 1β (IL-1β), macrophage inflammatory protein 1 alpha (MIP-1α), macrophage inflammatory protein 2 (MIP-2), tumor necrosis factor alpha (TNF-α), and monocyte chemoattractant protein 1 (MCP-1) (Fig. 1A). These cytokines were also induced upon insertion of MN alone, but their levels were further increased by immunization using MN coated with influenza vaccine. These levels were further enhanced at the 12-h time point. The increase of these cytokine expression levels has been demonstrated to contribute to the regulation of epidermal Langerhans cell migration and the subsequent accumulation of dendritic cells in the draining lymph nodes, in addition to their role in neutrophil and monocyte recruitment (19, 20).

The levels of other cytokines important for proliferation, activation, and recruitment of neutrophils and monocytes, such as granulocyte colony-stimulating factor (G-CSF), interferon gamma-induced protein 10 (IP-10), and cytokine-induced neutrophil chemoattractant (CXCL-1; also called CINC-1 or KC), were also increased by MN vaccination (Fig. 1B). Although the level of the important T helper 1 (Th1) chemokine IP-10 was increased statistically after MN delivery, IL-12 and gamma interferon, which characterize a Th1 response, were not found to be expressed at elevated levels in the skin. In addition, leukemia inhibitory factor (LIF), a cytokine induced by TNF-α and demonstrated to have an anti-inflammatory role in cutaneous inflammation (21), was modestly increased in the skin biopsy specimens after vaccination. Therefore, these findings indicate that a rapid increase of cytokines at the insertion site was induced by MN mechanical skin penetration, which was enhanced upon antigen delivery. The skin cytokine profile analysis shows that skin immunization induces a local innate immune response and a release of chemokines in the skin suggestive of the activation and recruitment of immune cells to the site of vaccination.

***In vivo* uptake and egress of labeled-influenza virus antigen after MN immunization.** To determine whether skin-resident dendritic cells were mobilized after MN vaccination, we assessed egress of cells from the ears of mice immunized with labeled (PR8-Qdot) or antigen-free MN by an *ex vivo* skin organ assay. In this assay, migrating cells exit the excised skin and collect in the medium, where their phenotype can be determined by flow cytometry. Following MN vaccination, we detected influenza antigen-positive cell emigrants in the medium from the ear explants within the first 2 h (Fig. 2). At 2 h, 50% of dendritic cells, characterized by the expression of the cell surface marker CD11c, were influenza antigen positive ($2.6 \times 10^3 \pm 0.6 \times 10^3$ $CD11c^+$ cells/explant). The 30-min time point showed the highest percentage of antigen-labeled cells; these represented 70% of the dendritic cells that had egressed ($6.6 \times 10^3 \pm 1.3 \times 10^3$). A population of CD11c-negative cells was also found to peak at 30 min and to contain labeled influenza virus antigen ($0.9 \times 10^3 \pm 0.1 \times 10^3$). Cells labeled with fluorescent influenza virus were not detected at later time points. These findings suggest that skin-resident dendritic cells capture antigen and rapidly migrate to the draining lymph nodes, where they present the antigen to naive lymphocytes. However, we did not identify the fluorescent influenza virus-loaded cells in the draining lymph nodes when we examined them in the first 3 days postimmunization.

In order to characterize the phenotype of the skin explant emigrants and to assess their maturation status, we used fluorescently labeled antibodies against CD40, major histocompatibility complex class II (MHC II), and CD86 for flow cytometry analysis. These markers have been associated with dendritic cell maturation and have been shown to be required for antigen presentation (22, 23). $CD11c^+$ cells that emigrated from the vaccinated skin showed high expression levels of the cell surface markers MHC II and CD205 and a low expression level of CD8 (Fig. 3A). In addition, more than 50% of these cells had increased expression of the costimulatory markers CD40 and CD86, characteristic of activated dendritic cells. Furthermore, 35% of these cells were positive for Qdot-labeled influenza virus (Fig. 3B). We were not able to detect any $CD11c^+$ $CD8^-$ $CD205^+$ cells that were positive for Qdot-labeled influenza virus (Fig. 3C). Expression of both CD40 and CD86 together with increased MHC class II expression suggests that these skin-derived dendritic cells are activated and mature (24). This phenotype is required for T cell priming, and such cells are likely to contribute to the strong immune response observed with MN vaccination.

***In vivo* whole-body fluorescence imaging of MN-immunized mice.** To noninvasively monitor the delivery of antigen to skin via MN delivery, mice were immunized with ovalbumin-Alexa Fluor 488 (OVA 488)-coated needles, and the kinetics of the protein retention in the skin were evaluated. The insertion site was monitored for 1 week, images were captured at 10 min and days 1, 2, 3, 5, and 8 after immunization, and the levels of protein fluorescence were compared over time. We observed an intense deposition of antigen corresponding to the site of microneedle array insertion

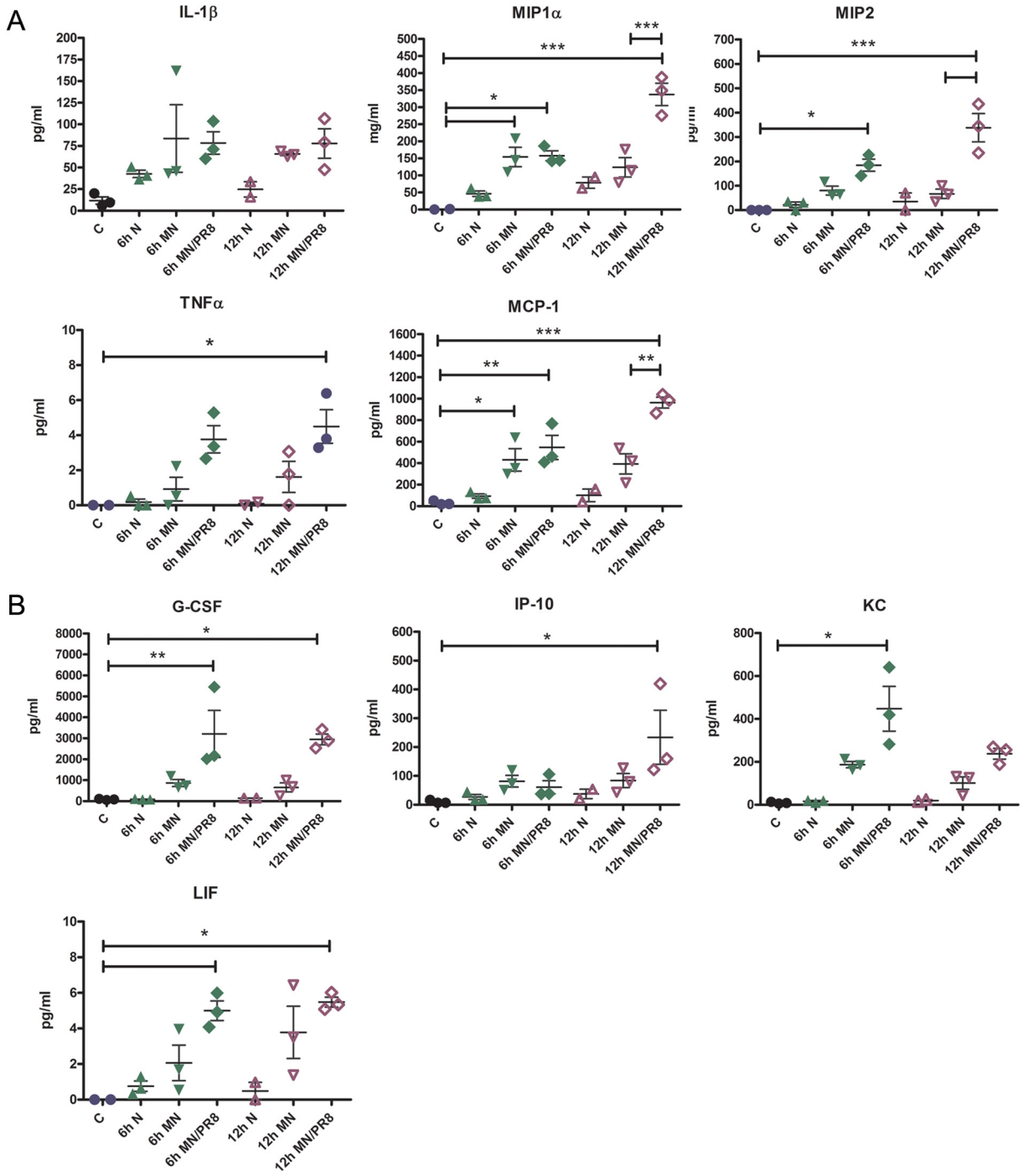

FIG 1 Inflammatory cytokine release after MN immunization with inactivated influenza virus. Skin samples were collected 6 h and 12 h after MN immunization with 3 μg of inactivated virus, and tissue lysates were evaluated for cytokine release by Luminex multiplex assay. The graphs show the concentrations of the cytokines that were differentially expressed for the following mouse groups: C, naive control; 6 h N, 6-h naive shaved; 6 h MN, 6-h MN mock; 6 h MN/PR8, 6-h PR8-coated MN; 12 h N, 12-h naive shaved; 12 h MN, 12-h MN mock; and 12 h MN/PR8, 12-h PR8-coated MN. Data are representative of two experiments, and data are means ± SD ($n = 3$). Asterisks indicate the statistical significance of selected comparisons: *, $P \leq 0.05$; **, $P \leq 0.01$; and ***, $P \leq 0.001$.

that could be detected for at least 5 days after delivery in the MN-immunized group when exposure settings were kept constant (see Fig. S1A in the supplemental material). The injection site of MN- or intramuscularly (IM)-delivered fluorescent OVA was detected using a PANSEE imaging system in the caudal dorsal region and ventral images of the quadriceps muscles, respectively. An IM-immunized group was used as a comparator for antigen dissipation after immunization. No signs of erythema, edema, or induration were observed at the sites of injection in any of the groups. The fluorescence intensity dissipated with time, but even at day 8,

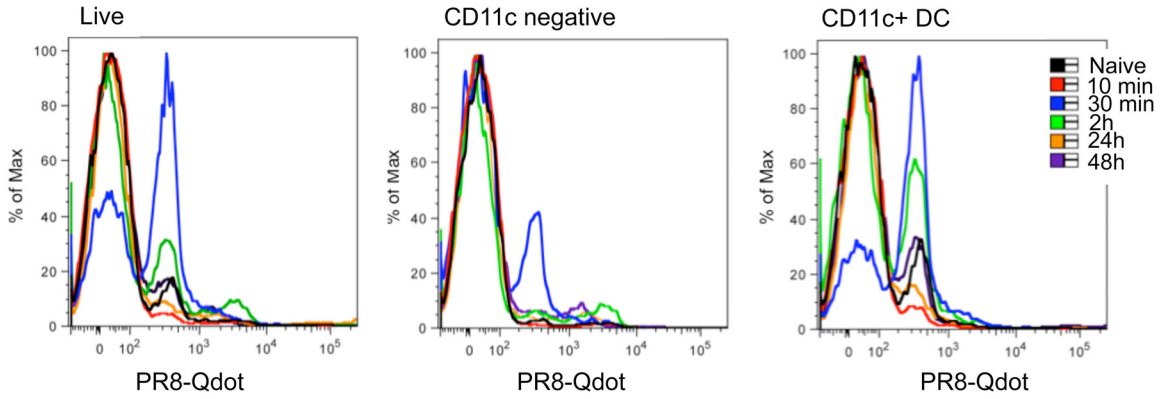

FIG 2 Transport of Qdot-labeled PR8 is primarily mediated by dermal dendritic cells. Qdot 655-labeled PR8 virus was used to coat MN and delivered into the skin in the ears of BALB/c mice. Auricular emigrants of explants were harvested from mice 10 min, 30 min, 2 h, 24 h, and 48 h postimmunization. Shown are representative flow cytometry analyses of Qdot-positive populations of total live cell emigrants, CD11c-negative cells, and dendritic cells ($CD11c^+$).

the antigen was still detected in skin exposed at a 4-fold-higher gain and 20% higher illumination (data not shown). Analysis of the integrated density revealed that 2 days following microneedle insertion, approximately half of the antigen remained at the injection site. The integrated intensity variation was more prominent between IM samples, possibly as a result of the antigen delivery as a suspension compared to the more localized antigen deposition by MN delivery. In addition, a slightly higher dissipation of the signal 3 days postvaccination was observed in the IM group. At day 3, similar levels of antigen were still observed in the skin. Approximately 2.5-fold more antigen was detected at the site of MN vaccination than at the site of IM vaccination (Table 1).

To confirm that the *in vivo* fluorescence signals of OVA accurately represented the localization of inactivated influenza vaccine and to improve the imaging detection level, inactivated virus was labeled with Qdot 705 nanocrystals (Qdot) and visualized with the CRi Maestro EX *in vivo* imaging system, which allows the detection of broader emission spectra. To more accurately represent the actual vaccine dose, 5 μg of inactivated labeled influenza virus was used to vaccinate the mice and commercially labeled streptavidin

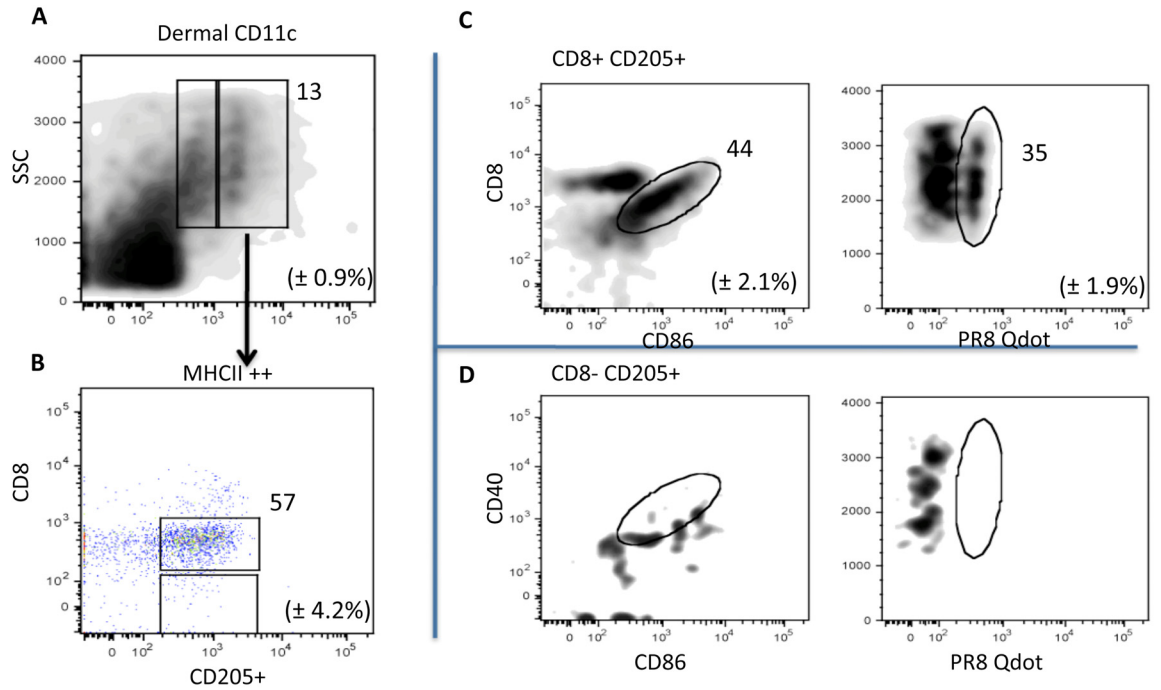

FIG 3 Dendritic cells draining from skin and bearing PR8-Qdot antigen exhibit a mature phenotype. Results of flow cytometry analysis of DC emigrants from auricular explants after MN vaccination are shown. (A) Cells were evaluated for the expression of MHCI class II (MHC II). (B) Highly MHC II-positive DC (MHC II++) showing a distinct population of $CD8^+$ $CD205^+$ DC. (C) Plots of the latter showing the expression of maturation markers CD40 and CD86 and the prominent population positive for the PR8-Qdot label. The SD from two experiments with 3 to 5 mice are shown. (D) Fraction of MHC II++ DC negative for CD8 expression.

TABLE 1 Tissue-integrated fluorescence density of labeled antigen

Group	Density (mean ± SD)[a]	%
MN		
d1	$5.8 \times 10^6 \pm 3.0 \times 10^6$	100
d2	$2.9 \times 10^6 \pm 0.5 \times 10^6$	50
d3	$3.2 \times 10^6 \pm 0.6 \times 10^6$	55
d5	$0.6 \times 10^6 \pm 0.1 \times 10^6$	10
d8	ND	
IM		
d1	$4.3 \times 10^6 \pm 2.8 \times 10^6$	100
d2	$2.4 \times 10^6 \pm 1.2 \times 10^6$	54
d3	$1.3 \times 10^6 \pm 0.4 \times 10^6$	28
d5	$0.3 \times 10^6 \pm 0.3 \times 10^6$	7
d8	ND	

[a] The signal intensity was quantified using ImageJ software at the injection site from images captured day 0 through day 8 after MN delivery or IM injection. ND, signal was below detection level.

Alexa Fluor 750 was used as a positive control. Images of MN-immunized mice were captured immediately after vaccination and at days 1, 2, 3, 7, 14, and 21 after vaccination (Fig. 4A and B). A concentrated deposition of antigen was observed at the site of insertion that decreased approximately 4-fold by day 3 but was still detectable at day 14 when skin was exposed for a longer period. In order to visualize the insertion site, the exposure time was doubled for each of the mouse groups evaluated (2× = 2,000 ms for $d7^a$-$d21^a$ (Fig. 4A) and $d3^b$-$d21^b$ (Fig. 4B) mice). The streptavidin-Alexa 750-treated mice also showed a similar pattern of antigen deposition with a slightly higher rate of decrease (Table 2) than the labeled inactivated virus, as indicated by the residual fluorescence at the site of injection. The slow release of inactivated influenza virus antigen from the skin correlates with the results observed with OVA as a model antigen and supports the conclusion that MN delivery results in prolonged deposition of antigen in the skin.

DISCUSSION

Influenza vaccines with enhanced immunogenicity are needed to improve protection, particularly for individuals at high risk of influenza-related complications. One of the approaches to achieve this goal is the evaluation of new vaccine delivery routes. Although the efficacy of intradermal vaccination has been proven to be successful for vaccines such as those against bacillus Calmette-Guérin, smallpox, rabies and, most recently, influenza, it is not widely practiced for other vaccines (25). In recent studies, alternative delivery approaches designed to reach the dermal layer have demonstrated successful vaccine delivery and protective immune responses in animal models. In clinical studies, intradermal delivery of vaccine antigens, including influenza virus antigens, has shown promising results (26). The main obstacle to the use of the intradermal delivery route is the lack of an appropriate delivery system that could circumvent the technically difficult Mantoux technique. Some examples of techniques that penetrate or disrupt the outermost layer of the skin, the stratum corneum, rely on the use of hypodermic microneedles, sandpaper, or electrical current.

Previously we demonstrated that MN immunization produces robust serum antibody responses and cellular responses capable of conferring protection against viral challenge at least as effectively as most conventional immunization routes (27). Importantly, antibody titers remained elevated in the MN-immunized group even 6 months after vaccination and correlated with inhibition of viral replication and robust recall Th1 cellular responses after influenza virus challenge (28). Therefore, the immune responses observed after a single MN dose not only are potent but also provide long-term immunity.

In the present study, we evaluated the innate immune responses in the skin that precede the development of the influenza virus-specific responses in order to investigate the mechanism of vaccine-induced immunity. Keratinocytes make up approximately 90% of the total cell population of the skin and play an important role in the innate immune response by secreting cytokines, chemokines, and antimicrobial peptides in response to foreign antigen (11, 29, 30). Cross-talk between keratinocytes and Langerhans cells via these innate immune signals induces activation, maturation, and migration of antigen-presenting cells to draining lymph nodes. The importance of IL-1β and TNF-α in induction of Langerhans cell migration from the epidermis has been demonstrated in skin contact sensitization models and in experimental cutaneous *Leishmania* infections (31, 32). Our analysis of cytokine expression in the skin following insertion of antigen-coated microneedles indicates the upregulation of IL-1β, TNF-α, and MIP-1α and supports the current models of Langerhans cell migration. The induction of the chemotactic proteins MIP-1α, MIP-2, MCP-1, IP-10, G-CSF, and KC suggests that following antigen-coated microneedle vaccination, the production of IL-1β and TNF-α in the skin is reinforced by recruitment of neutrophils and macrophages to the site of vaccination (33). Further work is needed to determine if the cytokine pattern observed is antigen specific, and such studies might offer a predictive signature that could serve to rapidly evaluate novel vaccine formulations.

Previous studies have demonstrated the migration of antigen-loaded Langerhans cells from mouse skin and subsequent homing to draining lymph nodes (34). Such migration is important in priming naive lymphocytes and activation of the adaptive immune response. Here we have demonstrated the migration of activated and matured antigen-loaded $CD11c^+$ DC from vaccinated skin with antigen-coated microneedles. These antigen-loaded $CD11c^+$ DC also expressed low levels of CD8α and high levels of CD205, indicating that they were of skin origin (35, 36). In addition, these cells expressed high levels of MHC II and costimulatory molecules (CD86 and CD40), suggesting that they are capable of efficient activation of naive antigen-specific T lymphocytes. These results are consistent with previous studies indicating increased expression of CD80 and CD86 in Langerhans cells migrating from murine skin explants (36, 37).

Macroimaging of mice vaccinated with Qdot-labeled influenza virus indicates that antigen is deposited in the skin for up to 7 days (Fig. 4). This prolonged deposition of antigen suggests the formation of "antigen depots" at the sites of microneedle insertion. Antigen depot formation leads to prolonged antigen release, allowing efficient uptake by antigen-presenting cells (38). Adjuvants such as aluminum hydroxide and incomplete Freund's adjuvant are capable of forming antigen depots in addition to inducing the production of proinflammatory cytokines and granulocyte-recruiting chemokines, further serving their roles as immunostimulants (39, 40). It will be of interest to determine if the rate of release of vaccine from an antigen depot might depend on the large size of the inactivated virus antigen and the kinetics of antigen trafficking to the draining lymph nodes. In addition, we have

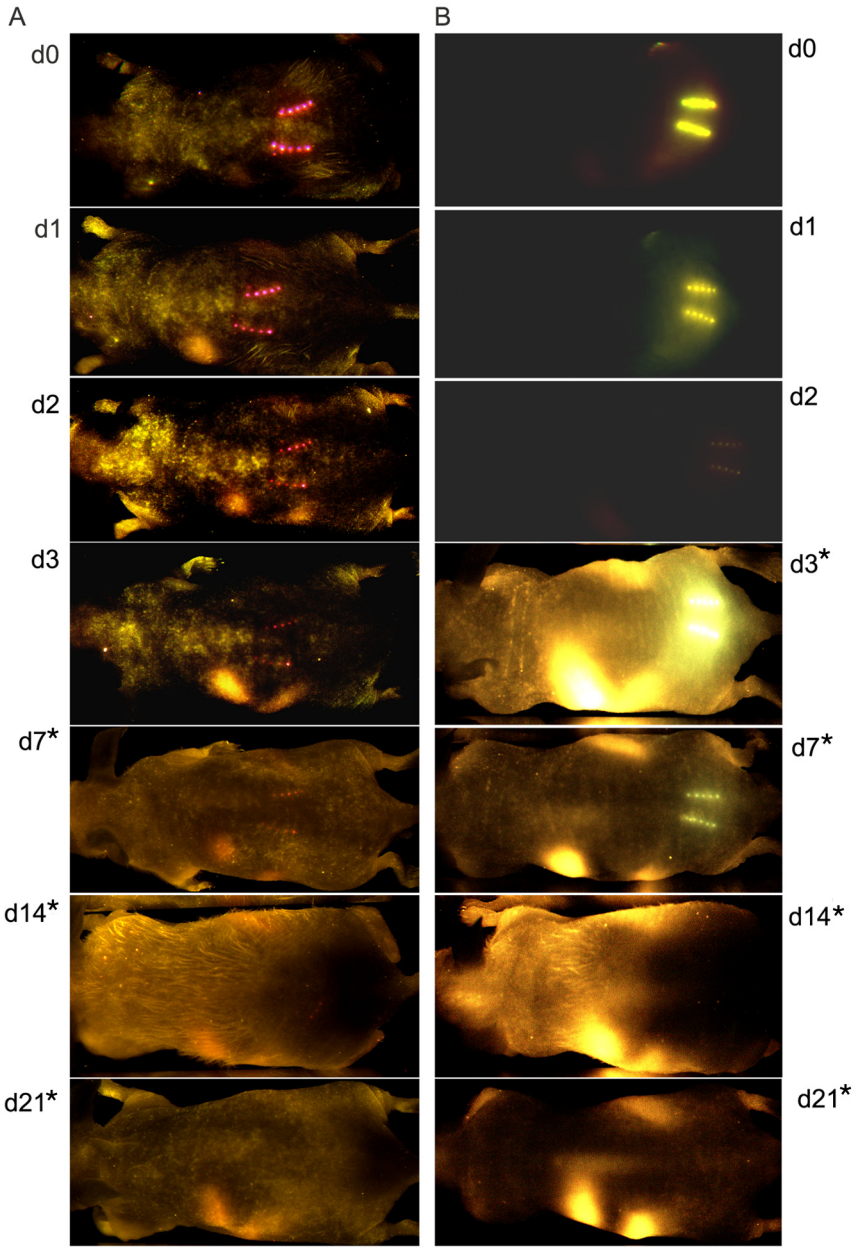

FIG 4 *In vivo* fluorescence imaging to measure antigen deposition after MN delivery. Kinetics of trafficking of (A) PR8 Qdot-labeled (PR8 Qdot) after MN vaccination and (B) MN-delivered streptavidin-Alexa 750. Images were captured at 10 min (d0) and days 1, 2, 3, 7, 14, and 21 after MN delivery. Representative images from three or four mice each in the PR8 Qdot and streptavidin-A750 groups are shown. *, indicates that the exposure time has been doubled.

shown that the local innate immune response is activated at the site of microneedle vaccination, resulting in the production of proinflammatory cytokines and chemokines. This early innate signaling induces activation and maturation of skin antigen-presenting cells, which have also captured antigen deposited by microneedle insertion. These cells migrate to draining lymph nodes, where they express CD40 and CD86 costimulatory molecules. Taken together, these results indicate that the efficiency of microneedle patch vaccination is controlled by the skin innate immune response and the migration of skin dendritic cell populations to the draining lymph nodes.

Using surface cell markers selected for murine DC characterization, CD205 and CD11c, we identified influenza virus-loaded DC and observed their migration from the skin, which suggests the capacity to travel to the lymph nodes. Our goal was to determine whether inactivated influenza virus used as a vaccine and delivered via MN was associated with skin dendritic cell maturation and to create parallels to research findings that have traditionally used fluorophores and ovalbumin as model antigens. This is of particular relevance in light of the differential T helper polarization observed at various skin immunization sites, correlating with site-specific DC distribution and dynamics (41).

With the kinetics of antigen distribution and its dependence on the antigen and immunization route having been characterized, it

TABLE 2 Integrated fluorescence density in the skin of MN-immunize mice

Group	Density (mean ± SD)[a]	%
Alexa 750		
d0	$22.90 \times 10^6 \pm 0.61 \times 10^6$	100
d1	$3.17 \times 10^6 \pm 0.67 \times 10^6$	14
d2	$1.89 \times 10^6 \pm 0.47 \times 10^6$	8
d3	$0.66 \times 10^6 \pm 0.19 \times 10^6$	3
d5	$0.15 \times 10^6 \pm 0.15 \times 10^6$	1
PR8-Qdot		
d0	$1.80 \times 10^6 \pm 0.46 \times 10^6$	100
d1	$0.75 \times 10^6 \pm 0.12 \times 10^6$	42
d2	$0.14 \times 10^6 \pm 0.05 \times 10^6$	8
d3	$0.13 \times 10^6 \pm 0.06 \times 10^6$	7
d5	$0.08 \times 10^6 \pm 0.01 \times 10^6$	4

[a] The signal intensity was quantified using ImageJ software at the injection site from images captured day 0 through day 5 after MN delivery.

will be of interest to investigate the different dendritic cell subpopulations involved in antigen presentation after inactivated-virus MN immunization. Moreover, the recent use of antibodies to target antigens to specific DC subsets has demonstrated the potential to enhance the magnitude of the adaptive immune response (42). The changes in specific innate cells and the skin cytokine profile generated after vaccination are important parameters in characterizing the mechanisms involved in responses to skin immunization.

MATERIALS AND METHODS

Microneedles. Solid metal microneedles were fabricated by etching stainless steel sheets (McMaster-Carr, Atlanta, GA) to measure 700 μm tall, with a cross-sectional area of 170 μm by 55 μm at the base and tapering to a sharp tip. The microneedles consisted of five needles per array. A coating solution was formulated with 1% (wt/vol) carboxymethylcellulose (Carbo-Mer, San Diego, CA), 0.5% (wt/vol) Lutrol F-68NF (BASF, Florham Park, NJ), and 15% (wt/vol) d-(+)-trehalose dihydrate (Sigma, St. Louis, MO). This coating solution contained inactivated A/Puerto Rico/8/34 (PR8) virus, fluorescently labeled PR8, ovalbumin-Alexa Fluor 488, or Alexa Fluor 750 (Invitrogen, Eugene, OR). Microneedles were coated as described previously (13).

Influenza virus. Influenza virus was grown in the allantoic cavities of chicken eggs, purified, and inactivated as described (43). To assess virus titers, hemagglutination (HA) activity was determined using chicken red blood cells (LAMPIRE Biological Laboratories, Pipersville, PA) and by a protein concentration assay (Bio-Rad Laboratories, Hercules, CA), as previously described (44). Inactivated PR8 virus was labeled using the EZ-link sulfo NHS-L-C biotin reagent (Thermoscientific, Rockford, IL) following the manufacturer's instructions, followed by labeling with streptavidin Qdot 655 or Qdot 705 (Invitrogen, Eugene, OR). To remove excess biotin and other reagents between steps, the samples were dialyzed against phosphate-buffered saline (PBS) overnight.

Immunizations. Emory University's Institutional Animal Care and Use Committee (IACUC) approved all animal procedures. Six- to eight-week-old female BALB/c mice (Charles River Laboratory, Wilmington, MA) and NCr nude mice (Taconic, Hudson, NY) were vaccinated with 10 μg of model antigen which had been used to coat MN arrays (inactivated labeled PR8 virus, ovalbumin-Alexa Fluor 488, or streptavidin-Alexa Fluor 750) or via the intramuscular (IM) route. MN immunization was performed in anesthetized mice, 48 h after dorsal caudal skin treatment with hair removal cream (Nair; Church & Dwight Co. Inc., Princeton, NJ). MN arrays were left inserted in the skin for 5 min to ensure that the coating antigen was delivered. Naive mice and mice receiving mock vaccination with MN lacking antigen were used as negative control groups.

Detection of skin cytokines. Skin surrounding the insertion site (approximately 0.5 cm^2) was dissected 6 or 12 h postimmunization and processed for tissue cytokine analysis as previously described (45). Cytokine analysis was performed using a mouse 31-plex Luminex cytokine assay at the BIIR Luminex Core (Dallas, TX).

Migration assays and flow cytometry. For migration assays, coated MN arrays were used to immunize mice on the dorsal ear surface. Ears were collected at 10 min, 30 min, 2 h, 24 h, and 48 h postimmunization and used to establish skin organ cultures. Murine ear skin explants were performed as previously described (46). Briefly, the ears were split into dorsal and ventral halves and placed in Transwell plates (Corning Inc., Lowell, MA) in RPMI supplemented with fetal calf serum and penicillin/streptomycin. Migratory cells were harvested 72 h later and washed in 1% bovine serum albumin in PBS. Cells collected from each Transwell plate, corresponding to one auricular tissue sample, were analyzed independently by surface staining with fluorochrome-conjugated anti-mouse CD11c, MHC class II, CD40, CD86, CD205, or CD8 antibodies purchased from eBioscience (San Diego, CA) or BD Bioscience Pharmingen (San Diego, CA). The data were acquired on a BD Biosciences LSRII flow cytometer and analyzed using FlowJo software (v6.3.3; Tree Star Inc., San Diego, CA).

***In vivo* fluorescence imaging.** Shaved mice were anesthetized with a ketamine-xylazine cocktail intraperitoneally and immunized with 25 μg of ovalbumin-Alexa Fluor 488 using coated MN or via IM injection. Images were obtained using the LT9-PANSEE panoramic imaging system (Lightools Research, Encinitas, CA) at 10 min, 24 h, 48 h, and 72 h. Ovalbumin 488 (OVA 488) was visualized using a green filter for excitation (470/40 nm) and 515 nm emission at an exposure time of 200 ms for MN and 400 ms for IM groups. Measurements of injection site integrated density were made by analyzing digital photographs using the software program ImageJ (NIH Research Services Branch, Bethesda, MD). Qdot 705-labeled virus (5 μg) or streptavidin Alexa Fluor 75-labeled MN-immunized nude mice were imaged using the CRi Maestro EX in vivo imaging system (Cambridge Research and Instrumentation, Woburn, MA). To capture the image for the Qdot 705 fluorochrome, the illumination filter was set on orange at 605 nm and the emission filter was set on yellow at 635 nm.

The filter settings in Alexa Fluor 750 experiments were deep red at 661 nm for the illumination filter and deep red at 700 nm for the emission filter. The spectral resolution for all imaging was 10 nm. Measurements of the injection site integrated intensity were made by analyzing digital photographs using the software Matlab version 2010a (MathWorks, Natick, MA).

Statistics. Data are given as means ± standard deviations (SD), and the number of animals per experimental group was three to five. Statistical significance was determined for grouped data by one-way analysis of variance with GraphPad Prism software. P values of ≤ 0.05 were considered significant.

ACKNOWLEDGMENTS

We thank Kiran Gill at the Emory Vaccine Center Flow Core for technical support. We acknowledge Lawrence Melsen for his direction and expertise using the PANSEE imaging system and the Center for Systems Imaging of Wesley Woods Health Center at Emory for assistance with imaging as well. The work was supported in part by U.S. National Institutes of Health grants AI074579, EB006369, and EB012495. M.P.M. was supported by a fellowship from NIH/NIAID HHSN266200700006C Center of Excellence for Influenza Research and Surveillance.

M.R.P. and V.Z. serve as consultants to companies, are founding share-holders of companies, and are inventors on patents licensed to companies developing microneedle-based products. This possible conflict of interest has been disclosed and is being managed by Georgia Tech and Emory University.

SUPPLEMENTAL MATERIAL

Supplemental material for this article may be found at http://mbio.asm.org/lookup/suppl/doi:10.1128/mBio.00012-12/-/DCSupplemental.

Figure S1, TIF file, 1.8 MB.

REFERENCES

1. **Monto AS.** 2010. Seasonal influenza and vaccination coverage. Vaccine **28**(Suppl. 4):D33–D44.
2. **Ampofo WK, et al.** 2012. Improving influenza vaccine virus selection. Report of a WHO informal consultation held at WHO headquarters, Geneva, Switzerland, 14–16 June 2010. Influenza Other Respi. Viruses, **6**(2): 142–152.
3. **Hannoun C, Megas F, Piercy J.** 2004. Immunogenicity and protective efficacy of influenza vaccination. Virus Res. **103**(1–2):133–138.
4. **Coudeville L, et al.** 2010. Relationship between haemagglutination-inhibiting antibody titres and clinical protection against influenza: development and application of a Bayesian random-effects model. BMC Med. Res. Methodol. **10**:18.
5. **Block SL, Toback SL, Yi T, Ambrose CS.** 2009. Efficacy of a single dose of live attenuated influenza vaccine in previously unvaccinated children: a post hoc analysis of three studies of children aged 2 to 6 years. Clin. Ther. **31**(10):2140–2147.
6. **Ambrose CS, Levin MJ, Belshe RB.** 2011. The relative efficacy of trivalent live attenuated and inactivated influenza vaccines in children and adults. Influenza Other Respi Viruses **5**(2):67–75.
7. **Centers for Disease Control and Prevention (CDC).** 2011. Prevention and control of influenza with vaccines: recommendations of the Advisory Committee on Immunization Practices (ACIP). Am. J. Transplant.. **11**(10):2250–2255.
8. **Ansaldi F, Durando P, Icardi G.** 2011. Intradermal influenza vaccine and new devices: a promising chance for vaccine improvement. Expert Opin. Biol. Ther. **11**(3):415–427.
9. **Frenck RW, Jr, et al.** 2011. Comparison of the immunogenicity and safety of a split-virion, inactivated, trivalent influenza vaccine (Fluzone®) administered by intradermal and intramuscular route in healthy adults. Vaccine **29**(34):5666–5674.
10. **Teunissen MB, Haniffa M, Collin MP.** 2012. Insight into the immunobiology of human skin and functional specialization of skin dendritic cell subsets to innovate intradermal vaccination design. Curr. Top. Microbiol. Immunol. **351**:25–76.
11. **Di Meglio P, Qin JZ, Nickoloff BJ, Prausnitz MR, Kang SM.** 2009. Skin immune sentinels in health and disease. Nat. Rev. Immunol. **9**(10): 679–691.
12. **Weldon WC, et al.** 2011. Microneedle vaccination with stabilized recombinant influenza virus hemagglutinin induces improved protective immunity. Clin. Vaccine Immunol. **18**:647–654.
13. **Koutsonanos DG, et al.** 2009. Transdermal influenza immunization with vaccine-coated microneedle arrays. PLoS One **4**(3):e4773.
14. **Quan FS, Kim YC, Compans RW, Prausnitz MR, Kang SM.** 2010. Dose sparing enabled by skin immunization with influenza virus-like particle vaccine using microneedles. J. Control. Release **147**(3):326–332.
15. **Song JM, et al.** 2010. Improved protection against avian influenza H5N1 virus by a single vaccination with virus-like particles in skin using microneedles. Antiviral Res. **88**(2):244–247.
16. **Fernando GJ, et al.** 2010. Potent immunity to low doses of influenza vaccine by probabilistic guided micro-targeted skin delivery in a mouse model. PLoS One **5**(4):e10266.
17. **Pulendran B.** 2007. Tolls and beyond—many roads to vaccine immunity. N. Engl. J. Med. **356**(17):1776–1778.
18. **Pulendran B.** 2004. Modulating vaccine responses with dendritic cells and Toll-like receptors. Immunol. Rev. **199**:227–250.
19. **Griffiths CE, Dearman RJ, Cumberbatch M, Kimber I.** 2005. Cytokines and langerhans cell mobilisation in mouse and man. Cytokine **32**(2): 67–70.
20. **Caux C, et al.** 2002. Regulation of dendritic cell recruitment by chemokines. Transplantation **73**(1 Suppl.):S7–S11.
21. **Zhu M, Oishi K, Lee SC, Patterson PH.** 2001. Studies using leukemia inhibitory factor (LIF) knockout mice and a LIF adenoviral vector demonstrate a key anti-inflammatory role for this cytokine in cutaneous inflammation. J. Immunol. **166**(3):2049–2054.
22. **Vermaelen KY, Carro-Muino I, Lambrecht BN, Pauwels RA.** 2001. Specific migratory dendritic cells rapidly transport antigen from the airways to the thoracic lymph nodes. J. Exp. Med. **193**(1):51–60.
23. **El Marsafy S, Bagot M, Bensussan A, Mauviel A.** 2009. Dendritic cells in the skin—potential use for melanoma treatment. Pigment. Cell. Melanoma Res. **22**(1):30–41.
24. **Sparber F, Tripp CH, Hermann M, Romani N, Stoitzner P.** 2010. Langerhans cells and dermal dendritic cells capture protein antigens in the skin: possible targets for vaccination through the skin. Immunobiology **215**(9–10):770–779.
25. **Kim YC, Prausnitz MR.** 2011. Enabling skin vaccination using new delivery technologies. Drug. Deliv. Transl. Res. **1**(1):7–12.
26. **Kenney RT, Frech SA, Muenz LR, Villar CP, Glenn GM.** 2004. Dose sparing with intradermal injection of influenza vaccine. N. Engl. J. Med. **351**(22):2295–2301.
27. **Kim YC, Park JH, Prausnitz MR.** Microneedles for drug and vaccine delivery. Adv. Drug Deliv. Rev., in press.
28. **Koutsonanos DG, et al.** 2011. Serological memory and long-term protection to novel H1N1 influenza virus after skin vaccination. J. Infect. Dis. **204**(4):582–591
29. **Bal SM, Ding Z, van Riet E, Jiskoot W, Bouwstra JA.** 2010. Advances in transcutaneous vaccine delivery: do all ways lead to Rome? J. Control. Release **148**(3):266–282.
30. **Cumberbatch M, Dearman RJ, Griffiths CE, Kimber I.** 2000. Langerhans cell migration. Clin. Exp. Dermatol. **25**(5):413–418.
31. **Cumberbatch M, Dearman RJ, Kimber I.** 1997. Langerhans cells require signals from both tumour necrosis factor alpha and interleukin 1 beta for migration. Adv. Exp. Med. Biol. **417**:125–128.
32. **Arnoldi J, Moll H.** 1998. Langerhans cell migration in murine cutaneous leishmaniasis: regulation by tumor necrosis factor alpha, interleukin-1 beta, and macrophage inflammatory protein-1 alpha. Dev. Immunol. **6**(1–2):3–11.
33. **Croker BA, et al.** 2011. Neutrophils require SHP1 to regulate IL-1beta production and prevent inflammatory skin disease. J. Immunol. **186**(2): 1131–1139.
34. **Stoitzner P, Pfaller K, Stössel H, Romani N.** 2002. A close-up view of migrating Langerhans cells in the skin. J. Invest. Dermatol. **118**(1): 117–125.
35. **Shortman K, Liu YJ.** 2002. Mouse and human dendritic cell subtypes. Nat. Rev. **2**(3):151–161. doi: .
36. **Henri S, et al.** 2001. The dendritic cell populations of mouse lymph nodes. J. Immunol. **167**(2):741–748.
37. **Larsen CP, et al.** 1994. Regulation of immunostimulatory function and costimulatory molecule (B7-1 and B7-2) expression on murine dendritic cells. J. Immunol. **152**(11):5208–5219.
38. **Morefield GL, et al.** 2005. Role of aluminum-containing adjuvants in antigen internalization by dendritic cells *in vitro*. Vaccine **23**(13): 1588–1595. doi: .
39. **Bachmann MF, Jennings GT.** 2010. Vaccine delivery: a matter of size, geometry, kinetics and molecular patterns. Nat. Rev. **10**(11):787–796.
40. **Hem SL, Hogenesch H.** 2007. Relationship between physical and chemical properties of aluminum-containing adjuvants and immunopotentiation. Expert Rev. Vaccines **6**(5):685–698.
41. **Sen D, Forrest L, Kepler TB, Parker I, Cahalan MD.** 2010. Selective and site-specific mobilization of dermal dendritic cells and Langerhans cells by Th1- and Th2-polarizing adjuvants. Proc. Natl. Acad. Sci. U. S. A. **107**(18): 8334–8339.
42. **Caminschi I, Lahoud MH, Shortman K.** 2009. Enhancing immune responses by targeting antigen to DC. Eur. J. Immunol. **39**(4):931–938.
43. **Martin MDP, et al.** 2010. Adjuvanted influenza vaccine administered intradermally elicits robust long-term immune responses that confer protection from lethal challenge. PLoS One **5**(5):e10897.
44. **Compans RW.** 1974. Hemagglutination-inhibition: rapid assay for neuraminic acid-containing viruses. J. Virol. **14**(5):1307–1309.
45. **Barclay D, et al.** 2008. A simple, rapid, and convenient Luminex-compatible method of tissue isolation. J. Clin. Lab. Anal. **22**(4):278–281.
46. **Ortner U, et al.** 1996. An improved isolation method for murine migratory cutaneous dendritic cells. J. Immunol. Methods **193**(1):71–79.